Nanoscale Res Lett (2009) 4:828–833
DOI 10.1007/s11671-009-9323-9

NANO EXPRESS

Tin Oxide Nanowires: The Influence of Trap States on Ultrafast Carrier Relaxation

Andreas Othonos · Matthew Zervos · Demetra Tsokkou

Received: 31 January 2009 / Accepted: 14 April 2009 / Published online: 30 April 2009

Abstract We have studied the optical properties and carrier dynamics in SnO_2 nanowires (NWs) with an average radius of 50 nm that were grown via the vapor–liquid solid method. Transient differential absorption measurements have been employed to investigate the ultrafast relaxation dynamics of photogenerated carriers in the SnO_2 NWs. Steady state transmission measurements revealed that the band gap of these NWs is 3.77 eV and contains two broad absorption bands. The first is located below the band edge (shallow traps) and the second near the center of the band gap (deep traps). Both of these absorption bands seem to play a crucial role in the relaxation of the photogenerated carriers. Time resolved measurements suggest that the photogenerated carriers take a few picoseconds to move into the shallow trap states whereas they take $\sim$70 ps to move from the shallow to the deep trap states. Furthermore the recombination process of electrons in these trap states with holes in the valence band takes $\sim$2 ns. Auger recombination appears to be important at the highest fluence used in this study (500 $\mu J/cm^2$); however, it has negligible effect for fluences below 50 $\mu J/cm^2$. The Auger coefficient for the SnO_2 NWs was estimated to be $7.5 \pm 2.5 \times 10^{-31}$ cm^6/s.

A. Othonos (✉) · D. Tsokkou
Department of Physics, Research Centre of Ultrafast Science, University of Cyprus, P.O. Box 20537, 1678 Nicosia, Cyprus
e-mail: othonos@ucy.ac.cy

M. Zervos
Department of Mechanical and Manufacturing Engineering, Materials Science Group, Nanostructured Materials and Devices Laboratory, University of Cyprus, P.O. Box 20537, 1678 Nicosia, Cyprus

Keywords SnO_2 nanowires · Chemical vapour deposition · Carrier dynamics · Differential absorption spectroscopy

Introduction

Tin oxide (SnO_2) is considered an important wide-bandgap *n*-type semiconductor which has received a great deal of attention over the past few years due to its high transparency in the visible part of the spectrum and sensitivity to certain gases which make it technologically important for optoelectronic devices [1–6] and sensors [7]. In addition Sn is readily available and cheaper compared to indium (In) which is used for the growth of indium oxide (In_2O_3). Furthermore, in recent years, the field of semiconducting metal oxides has benefited a great deal from the development of one-dimensional nanostructures such as nanowires (NWs) and nanorods (NRs) due to their interesting properties arising from their small size [8, 9] and high surface-to-volume ratio. In view of this, there has been growing interest in the synthesis of SnO_2 NWs, the study of their fundamental electronic and optoelectronic properties, and finally device applications [10–13].

Despite the potential applications of SnO_2 NWs there has been no detailed study of the fundamental, ultrafast carrier relaxation mechanisms of the photogenerated carriers in this nanostructured material. Consequently, here we investigate the carrier dynamics in SnO_2 NWs and obtain a detailed understanding of the various relaxation mechanisms and the influence of trap states using transient white light absorption spectroscopy [14–16] with femtosecond resolution. We find that the band gap of the SnO_2 NWs is 3.77 eV and contains two broad absorption bands, the first of which is located below the band edge and is related to

shallow trap states while the second is near the center of the band gap due to deep trap states. Detailed transient measurements revealed their energetic position, carrier relaxation times, and the importance of Auger recombination.

Experimental Procedure

The SnO_2 NWs were grown using an atmospheric pressure chemical vapour deposition (APCVD) reactor which consists of four mass flow controllers (MFC's) and a horizontal quartz tube furnace, capable of reaching a maximum temperature of 1100 °C. Initially, approximately 0.2 g of fine Sn powder (Aldrich, <150 μm, 99.5%) was weighed and loaded into a quartz boat together with a square piece of Si(111) which was coated with 0.5 nm of Au. The Au layer was deposited via sputtering at a slow rate <5 Å/s using an Ar plasma under a pressure $<10^{-4}$ mBar. The sample was positioned a few mm downstream from the Sn and subsequently the boat was loaded into the reactor and positioned directly above the thermocouple used to measure the heater temperature at the centre of tube. After loading the boat at room temperature (RT), Ar (99.999%) was introduced at a flow rate of 500 standard cubic centimetres per minute (sccm) for 5 min in order to purge the tube.

Following this the temperature was ramped to 800 °C in an Ar flow of 100 sccm at a rate of 30 °C/min. Upon reaching T_G, the flow of Ar was maintained at 100 sccm for a further 90 min after which the tube was allowed to cool down over at least an hour in an inert gas flow of Ar, 100 sccm. The sample was removed only when the temperature was lower than 100 °C. For the optical measurements, NWs were grown directly onto square pieces of quartz that were coated with 0.5 nm of Au and had an area of $\approx 6 \times 6$ mm^2. The morphology of the SnO_2 NWs was examined with a TESCAN scanning electron microscope (SEM) while the crystal structure and the phase purity of the NWs were investigated using a SHIMADZU, XRD-6000, X-ray diffractometer, and Cu Ka source. A scan of θ–2θ in the range between 20° and 80° was performed for the SnO_2 NWs that were grown on Si(111) and quartz.

In this study, we investigate the ultrafast dynamic behavior of carriers in SnO_2 NWs following femtosecond pulse excitation through the temporal behavior of differential absorption [14–16]. The experimental study was carried out using an ultrafast amplifier system operating at 5 kHz. A self mode-locked Ti: Sapphire oscillator centered at 796 nm and generating 45 fs pulses was the source of short pulses. Approximately 1 mJ of amplified energy was used to pump an Optical Parametric Amplifier (OPA) providing ultrafast pulses in the UV range of the spectrum. The rest of the energy from the amplifier was used to generate 400 nm from a BBO crystal via second harmonic generation and white light super continuum. The UV femtosecond pulses from the OPA were used to excite the nanowires given that the expected band gap of this material is around 3.7 eV. A small part of the fundamental 796 nm pulses were used to generate VIS-IR super continuum light by focusing the beam on a 1 mm thick sapphire plate. Similarly a super continuum light in the UV region of the spectrum was also generated using 400 nm pulses. The white light probe beam was used in a pump-probe non-collinear geometry, with the pump beam been generated from the OPA. To minimize the broadening of the laser pulse, optical elements such as focusing mirrors were utilized in the setup. The reflected and transmission probe beams were separately directed onto their respective detectors after passing through a band pass filter and thus selecting the probe wavelength from the broad band white light. The differential reflected and transmission signals were measured using lock-in amplifiers with reference to the optical chopper frequency of the pump beam. The temporal variation in the photo-induced absorption was extracted using the transient reflection and transmission measurements, thus providing a means of monitoring the carrier dynamics within the probing region [14].

Results and Discussion

Tin oxide NWs have been grown so far by a variety of methods including thermal evaporation [17, 18], chemical vapour deposition [19], and the VLS method using carbothermal reduction of stannous oxide SnO at 880 °C for 90 min [20]. On the other hand, stannic oxide, SnO_2 NWs have been grown by direct oxidation of Sn at 900 °C under a flow of 10 sccm O_2 [21]. Similarly, Yang et al. obtained SnO_2 NWs at 900 °C under a flow of 50 sccm O_2 [22] while Wan et al. [23] obtained Sb doped SnO_2 NWs by heating up the mixture at 20 °C/min up to 900 °C under a flow of 500 sccm Ar with a trace of O_2. A typical scanning electron microscope (SEM) image of the SnO_2 NWs grown on quartz is shown in Fig. 1 where it is apparent that a large coverage has been obtained. The SnO_2 NWs have an average diameter of 50 nm and lengths ≥5 μms. Furthermore the diameter of the SnO_2 NWs was found to be uniform along their length. The growth of the SnO_2 NWs occurs via the formation of Au nanoparticles (NPs) from the thin layer of Au and the VLS mechanism. No NWs were obtained on Si(111) or quartz alone. In addition we have found that direct oxidation using a flow of O_2 during growth hinders the formation of SnO_2 NWs due to the oxidation of the Sn upstream, which melts at 232 °C and which in turn reduces the vapour pressure, especially at low temperatures i.e., $T \leq 800$ °C. While we obtained SnO_2 NWs at temperatures as low as 700 °C we find that the

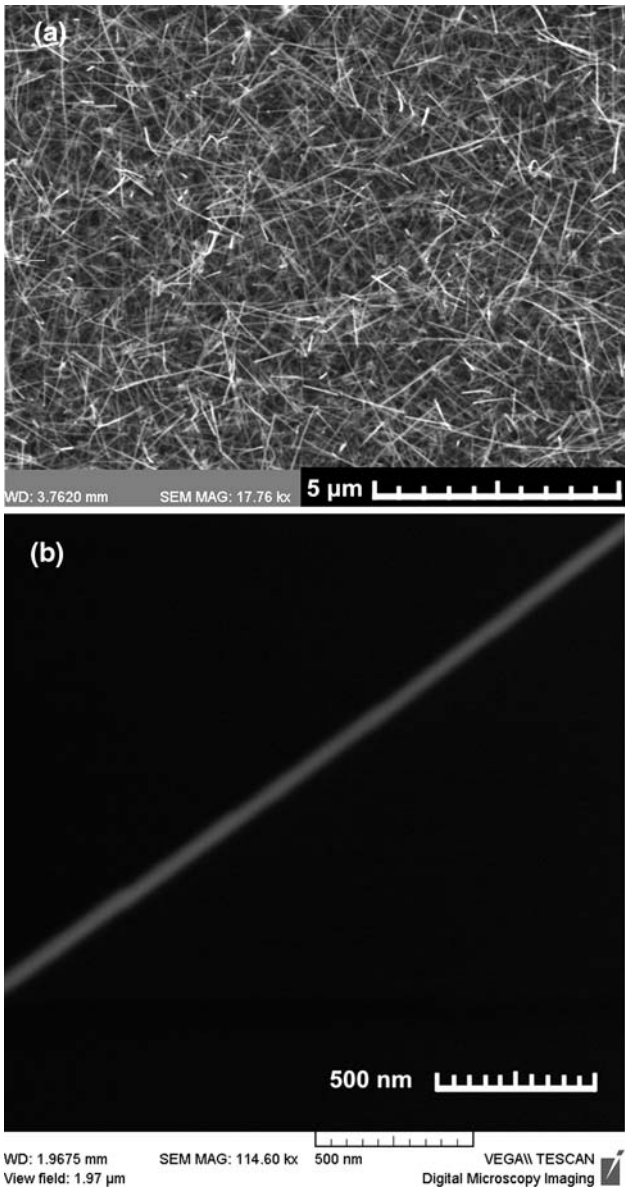

Fig. 1 SEM images of SnO_2 NWs grown at 800 °C with an average diameter of 50 nm

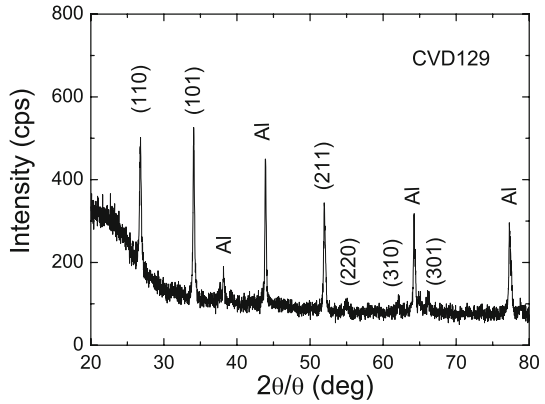

Fig. 2 XRD spectrum of the SnO_2 NWs grown at 800 °C on 0.5 nm Au/quartz

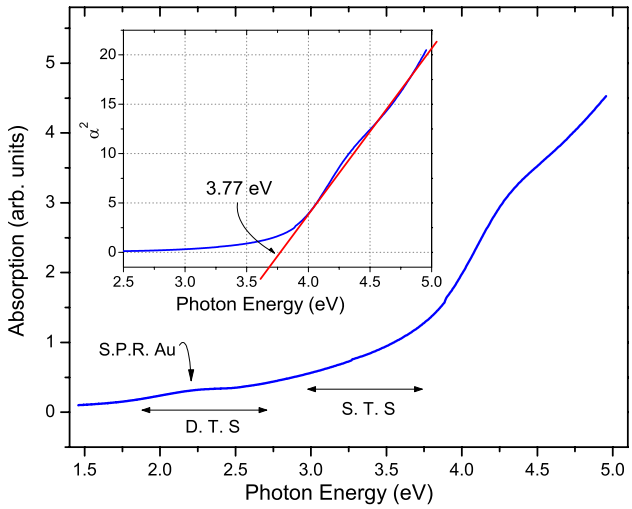

Fig. 3 Steady state transmission measurements carried out on SnO_2 NWs using a UV-IR spectrometer. The upper corner inset shows a plot of the square of the absorption versus incident photon energy, providing us with an estimate of the bandgap energy 3.77 eV. There are two broad absorption bands below the bandgap referred to as D.T.S—deep trap states and S.T.S.—shallow trap states

optimum temperature for a high yield and uniform coverage is 800 °C. The optimum growth conditions are therefore close to those described by Wan et al. [23] who use only a trace of oxygen under a larger flow of Ar i.e., 500 sccm as opposed to 100 sccm used here. In our case the formation of SnO_2 NWs is due to the oxygen admitted into the APCVD reactor at RT prior to the temperature ramp. The SnO_2 NWs grown at the optimum temperature i.e., $T_G = 800$ °C on quartz are characterized by the (1 1 0), (1 0 1), (2 1 1), (2 2 0), (3 1 0), and (3 0 1) peaks in the X-ray diffraction spectrum shown in Fig. 2. Diffraction peaks can be indexed to the tetragonal rutile structure of SnO_2 [22, 24]. We should point out that the Al peaks appearing in the XRD spectrum of Fig. 2 are due to the sample holder.

Following the growth of SnO_2 NWs, we performed steady state transmission measurements on the NWs grown on quartz. Figure 3 shows the optical absorption of the SnO_2 NWs covering a spectral range from the UV near to the IR. Given that SnO_2 is a direct gap semiconductor, a plot of the square of the absorption versus the incident photon energy provides a measure of the bandgap which was determined to be approximately 3.77 eV (see inset of Fig. 3). Here we should point out that there appears to be a broad absorption band around 4.2 eV which we believe to be due to lower lying valance bands [25]. In addition to

determining the energy bandgap, the absorption spectrum depicts several features within the energy gap of these NWs. There appears to be a broad absorption band below the band edge covering a range from 3.7 eV to 1.8 eV which may be divided into two regions [26, 27]. The first broad absorption band which starts just below the conduction-band edge of the NWs is associated with impurity traps and these are therefore commonly referred to as shallow trap states (S.T.S.). The second band is referred to as the deep trap states (D.T.S.) band generated by defects or/and surface imperfections. Both of these absorption bands seem to play a crucial role in the relaxation of photoexcited carriers on a femtosecond timescale. Furthermore, there appears to be a weak absorption band centred around 2.2 eV (see Fig. 3) which corresponds to the well known Surface Plasmon Resonance (S·P.R.) of Au nanoparticles that are required as catalysts for the formation of the SnO_2 NWs on quartz.

Figure 4 shows typical time resolved differential absorption measurements for the SnO_2 NWs excited at fluence of approximately 0.5 mJ/cm^2 with UV ultrafast pulses at 4.00 eV (310 nm) and probed at different photon probing energies ranging from UV to near IR. The *x*-axis on this graph corresponds to the optical delay between the pump and the probe pulse whereas the *y*-axis indicates the induced absorption. The behaviour appears to be complex and varies over the probing spectral range. For some of the probing wavelengths there is a sharp drop in the absorption reaching a minimum value and then followed by a slower recovery toward equilibrium that takes hundreds of pico-seconds, whereas in other cases there is a positive change in the absorption with again a recovery towards equilibrium.

These observed changes in absorption are associated with excitation of the SnO_2 NWs by photons whose energy is larger than the bandgap energy which results in the generation of non-equilibrium carriers. These non-equilibrium carriers will distribute themselves along energy states that are normally unoccupied under equilibrium conditions. The occupation of states (referred to as state filling) following an ultrafast laser pulse will appear as a reduction in the absorption at the probing energy states. Clearly the observed recovery of this negative absorption change will be a direct measure of the time required by the photogenerated carriers to move out of the occupied states. Furthermore, a positive change in the induced absorption is also observed in the transient absorption measurements. This phenomenon is mainly due to secondary excitation of the photo-generated carriers by the probing photons from their initial states to higher energy states. This "free-carrier absorption" depends on the number of carriers present at the initial states and the coupling coefficient between the two energy bands. The temporal profile of this positive induced absorption is again a direct measure of the presence of the photo-generated carrier at the probing energy states.

We will begin the analysis of the data from the degenerate induced absorption measurements where the excitation and probing photon energies were 4.00 eV. It is important to point out that the observed sharp drop reaching a minimum (state filling) is pulse width limited, which is expected since we are probing the same energy states that we are exciting. To obtain a better understanding of the dynamics for the degenerate pump-probe data, we have performed intensity measurements as seen in Fig. 5.

The normalized induced absorption measurements seen in Fig. 5 clearly indicate that with increasing fluence there is a faster recovery on the long time scale. This suggests that

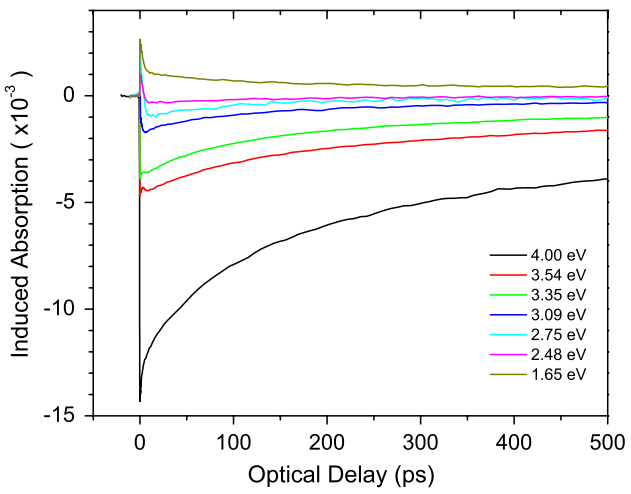

Fig. 4 Time-resolved differential absorption of SnO_2 nanowires excited with 4.00 eV photons (310 nm) at fluence of 500 μJ/cm^2 and probe at different photon energies ranging from UV to near IR

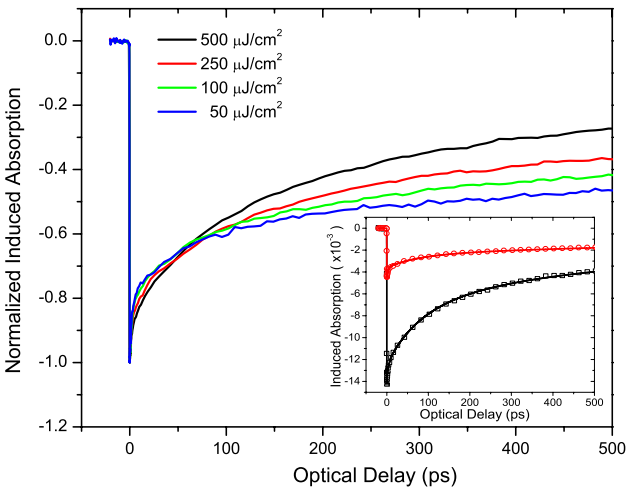

Fig. 5 Time-resolved normalized differential absorption intensity measurements of SnO_2 NWs excited with 4.0 eV and probe at 4.0 eV. The different curves correspond to different incident absorption fluence of the NWs. The inset shows the fits (*solid lines*) to the actual differential absorption data (*points*) using a simple model which includes multi-exponential decays and Auger recombination

Auger recombination is a contributing factor at the fluence used in this study. With decreasing fluence, Auger recombination becomes less important, and for the NWs used in this study at fluence less than 50 μJ/cm^2, this contribution may be considered negligible. A simple multi-exponential fit to the experimental result at 50 μJ/cm^2 shows that a minimum requirement of three exponential function is necessary for a good fit to the data. The time constants obtained from this fit were 2.4 ps (18%), 68 ps (22%), and 2.3 ns (60%). A more detailed analysis of the experimental data was performed using a simple differential equation model which incorporated the above three exponential decay mechanisms along with Auger recombination. Making use of the time constants obtained for the lowest fluence utilized in these experiments, where Auger recombination was negligible, it was possible to obtain fits to the differential absorption data at higher fluences. Relative good fits to the experimental data (see inset Fig. 5) were obtained using an Auger coefficient of $7.5 \pm 2.5 \times 10^{-31}$ cm^6/s.

A schematic diagram of the various proposed relaxation paths is shown in Fig. 6, to help the reader obtain a clear picture of the dynamics. The first time constant (2.4 ps) listed above, corresponds to mechanism 1, (see Fig. 6) whereas the second time constant is associated with mechanism 2 or 3 through carrier saturation in the shallow trap states. Given that no direct recombination was observed from the conduction to the valence band which is corroborated by the absence of photoluminescence near 3.75 eV, we

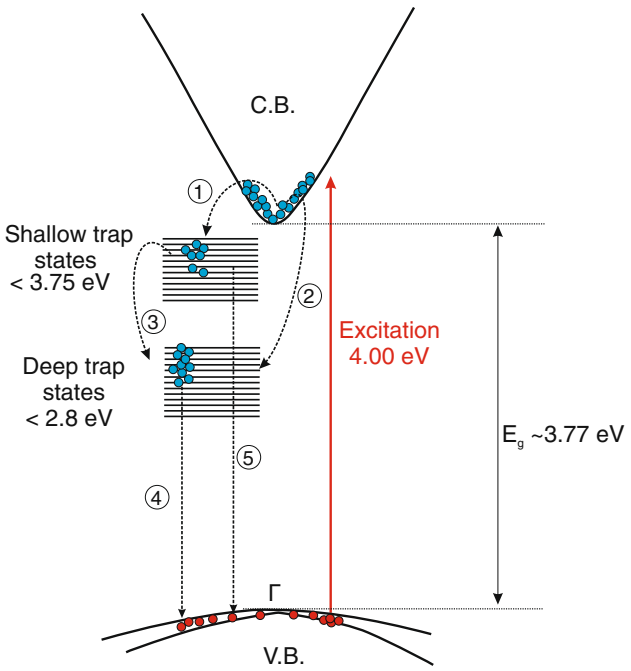

Fig. 6 A schematic diagram of the energy band gap diagram of SnO_2 NWs with the various relaxation mechanisms following carrier photoexcitation by an ultrafast pulse

believe that the long time constant is associated with the carriers moving through the shallow and deep trap states. Saturation of these states from the large number of carriers will result in the decay of paths 4 and/or 5 being effectively seen when probing above the band gap.

We should also point out that the fast decay component, which is associated with mechanism 1 of the photo-generated carriers when they are moving into the shallow traps states, appears to become slower with increasing fluence (Fig. 5). This is most likely due to saturation of available shallow trap states. Furthermore, in the above proposed model, the holes generated near the Γ point will also relax to the top of the valence band. However, the expected relaxation within the valence band is much faster than the multi-picosecond relaxation mechanisms shown in Fig. 6. This is expected given the small excess kinetic energy received by the holes during excitation.

Considering next the time-resolved absorption measurements (Fig. 4) for probing photon energies below the band gap energy (shallow traps) from 3.54 eV (350 nm) to 3.3 eV (380 nm), we notice that although the maximum state filling occurs very close to $t = 0$ (within the pulse width), there appears to be a small drop and then a small rise after a few picoseconds. This behavior is due to a small free-carrier contribution which reduces the state filling contribution thus artificially making this feature ("dip") appear near the tip of the maximum signal. This is clearly obvious when looking at the differential absorption in Fig. 4 with decreasing probing photon energy. The free-carrier "dip" increases with increasing probing wavelength and eventually becomes the main contributing factor at the longer probing wavelengths.

Furthermore, intensity measurements carried out over a range of 500–50 μJ/cm^2 at the probing photon energy of 3.54 eV (350 nm) indicate that Auger recombination has a noticeable effect only at the maximum fluence, however, at fluence as low as ~50 μJ/cm^2, this effect becomes negligible. A multi-exponential fit to the data shows a minimum requirement of two exponential function for a good fit with time constants of 72 ps (27%) and 2.08 ns (73%). Most likely the fast time constant is associated with carriers moving into the deep traps (path 3 in Fig. 6) whereas the long decay is associated with recombination of the carriers (path 5 in Fig. 6). Here we should point out that differential absorption intensity measurements have also been carried at other probing photon energies within the top shallow trap states with similar results.

Considering the differential absorption measurements in Fig. 4 for the longer probing wavelengths, we notice an increase in free-carrier contribution. This contribution becomes dominant for probing photon energies below 1.65 eV (750 nm), where no trap states can be reached from the valence band thus excluding state filling. The initial fast recovery component which is of the order of a

few picoseconds seen in these measurements is attributed to free-carrier contributions within the trap states.

Finally we should point out that due to the presence of Au nanoparticles (NPs) which are required as a catalysts in the formation of the SnO_2 NWs, transient absorption measurements in the probing region 2.4–2.1 eV depict the well known surface plasmon resonance of Au [28–30]. Time resolved measurements outside the above probing spectral region show no evidence of differential absorption signal from Au. Furthermore, measurements with excitation photons having energy below the band gap of SnO_2 show signal only at the probing region of the surface plasmon resonance. Identical results were obtained when transient absorption measurements were carried out on just the quartz substrate coated with the 0.5 nm film of the Au catalyst. It appears that the Au NPs required for the formation of the NWs have no effect on probing the carrier dynamics in SnO_2 NWs despite the strong plasmon resonance.

In conclusion, we have investigated the ultrafast dynamic behavior of SnO_2 nanowires using above band gap excitation UV femtosecond pulses. Transmission measurements of the NWs provided us with an estimate of the band gap at 3.75 eV and reveal broad absorption bands below the band edge. These absorption bands appear to play an important role in the relaxation of the photogenerated carriers in the NWs. Transient differential absorption measurements reveal the different pathways and time constants associated with the relaxation of the photogenerated carriers. Measurements suggest that the photogenerated carriers take a few picoseconds to move into the shallow traps states whereas it takes $\sim$70 ps to move from the shallow to the deep trap states. Furthermore, recombination of electrons from these traps states with holes in the valence band takes $\sim$2 ns. Auger recombination has a contribution to the carrier dynamics at the highest fluence used in this study ($\sim$500 μJ/cm^2), however at fluence of 50 μJ/cm^2 Auger recombination appears to be negligible. Transient absorption intensity measurements provided us with an estimate of the Auger coefficient for the SnO_2 NWs to be approximately $7.5 \pm 2.5 \times 10^{-31}$ cm^6/s.

Acknowledgments The study in this article was partially supported by the research programs; EPYNE/0504/06, ERYAN/0506/04, and ERYNE/0506/02 funded by the Cyprus Research Promotion Foundation in Cyprus.

References

1. Z.M. Jarzebski, J.P. Marton, J. Electrochem. Soc. **123**, 1990 (1976)
2. J. Maier, W. Gopel, J. Solid State Chem. **72**, 293 (1988). doi:10.1016/0022-4596(88)90032-1
3. K.P. Kumar, A.D. Domodaran, J. Mater. Sci. **24**, 220 (1989). doi:10.1007/BF00660957
4. S.A. Pianaro, P.R. Bueno, E. Longo, J.A. Varela, J. Mater. Sci. Lett. **14**, 692 (1995). doi:10.1007/BF00253373
5. P.I. Rovira, R.W. Collins, J. Appl. Phys. **85**, 2015 (1999). doi:10.1063/1.369496
6. N. Amin, T. Isaka, A. Yamada, M. Konagai, Sol. Energy Mater. Sol. Cells **67**, 195 (2001). doi:10.1016/S0927-0248(00)00281-6
7. N. Yamazoe, Sens. Actuators B Chem. **5**, 7 (1991). doi:10.1016/0925-4005(91)80213-4
8. Z.W. Pan, Z.R. Dai, Z.L. Wang, Science **291**, 1947 (2001). doi:10.1126/science.1058120
9. J. Zhang, J. Liu, J.L. Huang, P. Kim, C.M. Lieber, Science **274**, 757 (1996). doi:10.1126/science.274.5288.757
10. Z.R. Dai, J.L. Gole, J.D. Stout, Z.L. Wang, J. Phys. Chem. B **106**, 1274 (2002). doi:10.1021/jp013214r
11. Z. Liu, D. Zhang, S. Han, C. Li, T. Tang, W. Jin, X. Liu, B. Lei, C. Zhou, Adv. Mater. **15**, 1754 (2003). doi:10.1002/adma.200305439
12. X.C. Jiang, Y.L. Wang, T. Herricks, Y.N. Xia, J. Mater. Chem. **14**, 695 (2004). doi:10.1039/b313938g
13. M.J. Zheng, G.H. Li, X.Y. Zhang, S.Y. Huang, Y. Lei, L.D. Zhang, Chem. Mater. **13**, 3859 (2001). doi:10.1021/cm010084q
14. A. Othonos, J. Appl. Phys. **83**, 1789 (1998). doi:10.1063/1.367411
15. A. Othonos, E. Lioudakis, U. Philipose, H.E. Ruda, Appl. Phys. Lett. **91**, 241113 (2007). doi:10.1063/1.2825290
16. A. Othonos, M. Zervos, M. Pervolaraki, Nanoscale Res. Lett. **4**, 122 (2009). doi:10.1007/s11671-008-9211-8
17. M.S. Arnold, P. Avouris, Z.W. Pan, Z.L. Wang, J. Phys. Chem. B **107**, 659 (2003). doi:10.1021/jp0271054
18. X.Y. Xue, Y.J. Chen, Y.G. Liu, S.L. Shi, Y.G. Wang, T.H. Wang, Appl. Phys. Lett. **88**, 201907 (2006). doi:10.1063/1.2203941
19. S. Mathur, S. Barth, H. Shen, J.-C. Pyun, U. Werner, Small **1**, 713 (2005)
20. A. Kar, J. Yang, M. Dutta, M.A. Stroscio, J. Kumari, M. Meyyappan, Nanotechnology **20**, 065704 (2009). doi:10.1088/0957-4484/20/6/065704
21. Y.J. Ma, F. Zhou, L. Lu, Z. Zhang, Solid State Commun. **130**, 313 (2004). doi:10.1016/j.ssc.2004.02.013
22. M.-R. Yang, S.-Y. Chu, R.-C. Chang, Sens. Actuators B **122**, 269 (2007). doi:10.1016/j.snb.2006.05.034
23. Q. Wan, E.N. Dattoli, W. Lu, Appl. Phys. Lett. **90**, 222107 (2007). doi:10.1063/1.2743746
24. M. Chen, X. Xia, Z. Wang, Microelectron. Eng. **85**, 1379 (2008). doi:10.1016/j.mee.2008.01.027
25. F.J. Arlinghaus, J. Phys. Chem. Solids **35**, 931 (1974). doi:10.1016/S0022-3697(74)80102-2
26. R. Liu, Y. Chen, F. Wang, L. Cao, A. Pan, G. Yang, T. Wang, B. Zou, Physica E **39**, 223 (2007). doi:10.1016/j.physe.2007.04.009
27. D. Maestre, A. Cremades, J. Piqueras, J. Appl. Phys. **95**, 3027 (2004). doi:10.1063/1.1647267
28. A. Devizis, V. Vaicikauskas, V. Gulbinas, Appl. Opt. **45**, 11 (2006). doi:10.1364/AO.45.002535
29. S. Link, C. Burda, Z.L. Wang, M.A. El-Sayed, J. Chem. Phys. **111**, 3 (1999). doi:10.1063/1.479310
30. T.S. Ahmadi, S.L. Logunov, M.A. El-Sayed, J. Phys. Chem. **100**, 20 (1996). doi:10.1021/jp960484e